# Application of beamforming methods to full-scale military jet noise

Blaine M. Harker, Kent L. Gee, Tracianne B. Neilsen
*Brigham Young University, Department of Physics and Astronomy*
*N283 ESC, Provo, UT 84601, USA*

**Over the past decade, beamforming in aeroacoustics applications have undergone significant advances. Cross beamforming methods improve upon traditional beamforming in that they relax the assumption of multiple-source incoherence. This paper compares the abilities of three cross beamforming methods to reproduce source and field characteristics for an extended, partially correlated source that mimics supersonic jet noise radiation. Standard cross beamforming and two related methods that involve regularization—the hybrid method and improved generalized inverse beamforming—are applied to a numerically generated dataset along a near-field line. Estimated levels and coherence lengths are compared with benchmarks at the source as well as near and far-field locations. All three methods are successful in reproducing the field and source properties in high-amplitude regions. Although regularization generally helps to improve both source and field reconstructions, results are sensitive to regularization parameters, particularly for the generalized inverse method. The successful application of the three methods demonstrate the utility of cross-beamforming in formulating equivalent source models for accurate field prediction of complex sources, including jet noise.**[*]

## 1 INTRODUCTION

Reduction efforts of jet and rocket noise require an improved understanding of the noise source characteristics, which have been an active and perplexing topic of research for over six decades. While significant progress has been made towards increased understanding, a complete model describing source and field behavior does not exist. This has application to aerospace research, where next generation fighter jets demand improved power and performance and result in increased radiated sound fields. The current sound exposure levels to military [2] and aircraft personnel as well as community noise near airports fuels a need to better understand and mitigate the high sound levels.

Aeroacoustics studies have utilized many applications of beamforming techniques where sources are effectively modelled as incoherent monopoles [3, 4]. However, more complicated sources, such as those found in jet noise, violate traditional beamforming assumptions and additional considerations are necessary [5, 6]. Recent improvements to beamforming techniques over the past decade have allowed for the characterization of extended, partially correlated sources which span multiple wavelengths [7]. In addition, the beamforming results have been used as equivalent source models to predict far-field sound levels [5]. However, prior work has not examined the ability of the resultant source models to produce the correct coherence properties of the sound field. In this study, coherence properties and sound level predictions from three beamforming methods are compared, i.e., cross beamforming [8], the hybrid method [9], and improved generalized inverse beamforming [5], to quantify the performance of each method in obtaining an equivalent source distribution.

Prior beamforming studies have successfully been applied to extended, partially correlated sources. Venkatesh *et al.* [10] used a spatial integral approach to beamforming jet noise. Brooks and Humphreys [8] developed DAMAS-C, an extension of DAMAS [4] in which cross beamforming results are deconvolved to reduce array effects. This method has been applied to full-scale tactical jet noise sources to estimate correlated jet noise source distributions [11]. Padois *et al.* [9] developed the hybrid method, which applies a type of Tikhonov regularization customized to more accurately converge on physically meaningful distributed source estimates, and showed the regularization led to improvements over other methods when applied to full-scale jet noise. Dougherty [5] improved upon a similar method introduced by Suzuki [12], called generalized inverse beamforming, which uses a pseudo inverse and regularization to estimate a coherent, distributed source region. He used beamforming source estimates of noise from model-scale jets to predict far-field radiation levels and compared them with theoretical

[*] Portions of this research were presented at the 2016 Berlin Beamforming Conference [1]

expectations. Du and Morris [13] developed an equivalent source model of simulated jet noise by applying delay-sum beamforming to acoustic signals from a far-field polar array. The resulting equivalent source distribution at the jet centreline was analysed with proper orthogonal decomposition to obtain a wavepacket-like representation of the source. The work of the past decade improving beamforming methods for extended, partially correlated sources has been significant, yet, there is a need to carefully compare the performance of the different methods, particularly when using the beamforming results as an equivalent source model to generate the corresponding acoustic field properties.

In this study, cross beamforming (CBF), the hybrid method (HM), and improved generalized inverse beamforming (GINV) are described and applied in a numerical study to determine the capabilities and limitations of each when estimating the level and coherence properties of an extended, partially correlated source distribution and its resultant field. Each method is described in Section 2, along with a multiple-wavepacket source distribution designed to reproduce features of a jet noise field. The numerical case study is used to compare the capability of each method to obtain estimates of the source levels and coherence properties in Section 3. Resultant equivalent sources are used to predict the near and far-field levels and coherence properties, which are then compared with the numerical benchmark. An understanding of the efficacy of each method to generate an equivalent source distribution that accurately predicts the radiation levels and coherence characteristics in benchmark cases leads to improved understanding of the behaviour of these methods when applied to unknown sources, such as full-scale jet noise [7].

## 2 Methods

Unlike traditional far-field beamforming methods where the distance from source to array is much larger than the array size, beamforming in the geometric near field can lead to improved resolution [4]. However, the level of improvement is determined by the choice of reconstruction locations, the array geometry and dimensions relative to the source size, and the frequency under consideration. In this study, the array design is chosen to be sufficiently dense to produce high-resolution estimates of the source distribution without the need for deconvolution methods. In addition, the array spans the source region such that resolution across the source region is fairly uniform. The advanced beamforming methods compared in this study produce both level and coherence information across the source region, and these results can be used as an equivalent source model to estimate the radiated field. A brief summary of each beamforming method is presented, and changes in implementation and regularization choices are discussed.

### 2.1 Cross Beamforming

Cross beamforming is an extension of traditional beamforming that is capable of identifying source coherence characteristics. An array consisting of $M$ microphones is used to measure the pressure field, $\hat{p}(\vec{x}_m)$, at each array element location, $\vec{x}_m$, and for a given frequency, $f$ (which is not explicitly referenced for convenience). If we assume that $S$ sources, each with a complex source strength of $q(\vec{x}_s)$, are located at positions $\vec{x}_s$, we can describe the acoustic pressure in matrix form as

$$\hat{p}(\vec{\mathrm{x}}_m) = G(\vec{\mathrm{x}}_m, \vec{x}_s) q(\vec{x}_s). \quad (1)$$

Here, the free-field Green function, $G(\vec{x}_m, \vec{x}_s)$, incorporates the propagation from the source to the measurement location. Equation (1) can conveniently be rewritten in matrix format, such that

$$\mathbf{p} = \mathbf{G}\,\mathbf{q}, \quad (2)$$

where the vector of acoustic pressures, $\mathbf{p}$, is $[M, 1]$ in length, the vector of complex source strengths, $\mathbf{q}$, is $[S, 1]$. The Green function matrix, $\mathbf{G}$, is $[M, S]$ in size and accounts for the free-field propagation from each source to each array element. We seek to solve for $\mathbf{q}$, which is accomplished by solving a similar inverse problem:

$$\mathbf{q} = \mathbf{W}^{\mathrm{H}}\mathbf{p}, \quad (3)$$

where H is the conjugate transpose operator. The operator, $\mathbf{W}^{\mathrm{H}}$, is the steering vector matrix that can be formulated in several ways. In the traditional matrix beamforming methods, $\mathbf{W^H = G^H}$ [14]. As an alternative approach, various steering vector methods have been proposed that are designed enhance various aspects of source characteristics [15]. The definition in [14] is used in the present study; the resulting cross beamforming (CBF) response follows as

$$\mathbf{Q_{CBF} = qq^H = W^H pp^H W = W^H C W}, \quad (4)$$

where the quantity $\mathbf{C \equiv pp^H}$ is the cross-spectral matrix corresponding to the acoustic measurements. $\mathbf{Q_{CBF}}$ is a cross-spectral matrix of the source reconstruction estimated by the cross beamforming, and diagonal elements of $\mathbf{Q_{CBF}}$ contain the individual source powers commonly reported in conventional beamforming. The off-diagonal elements of $\mathbf{Q_{CBF}}$ are referred to as the cross beamforming elements and represent the simultaneous steering of the array pressures to two locations along the source region. The magnitude of the estimated cross beamforming

response, $Q_{\mathrm{CBF}}(\vec{x}_{s_1}, \vec{x}_{s_2})$, relative to the corresponding individual source responses [$Q_{\mathrm{CBF}}(\vec{x}_{s_1}, \vec{x}_{s_1})$ and $Q_{\mathrm{CBF}}(\vec{x}_{s_2}, \vec{x}_{s_2})$], is large if there exists a degree of coherence between corresponding source locations, $\vec{x}_{s_1}$ and $\vec{x}_{s_2}$. Techniques, such as DAMAS-C, rely on the cross beamforming response to model sources that exhibit some degree of mutual coherence but also apply a deconvolution technique to account for array artifacts [8]. In this instance, the array geometry was chosen such that the addition of deconvolution should not improve the source resolution.

### 2.2 The Hybrid Method

The hybrid method (HM) provides improved capabilities over conventional beamforming by using a modified regularization technique to constrain the beamforming results in such a way as to uniquely solve a problem [5, 9]. Regularization helps to mitigate the consequences of the underdetermined nature of this inverse problem. For example, it is commonly employed to define a measurement noise floor and suppress low-level values that may not be significant to the source reconstruction. A common regularization approach used in acoustical holography and related inverse methods is called Tikhonov regularization [9], in which a penalization parameter is added to the pseudo inverse of the Green function to improve the matrix conditioning by reducing the effects of measurement noise. The solution to Eq. (2) then becomes

$$\mathbf{q} = (\mathbf{G^H G} + \nu^2 \mathbf{L^H L})^{-1} \mathbf{G^H p}, \tag{5}$$

where $\nu^2$ is the penalization parameter, and $\mathbf{L}$ is a square weighting matrix. In classical Tikhonov regularization, $\mathbf{L}$ is set to be the identity matrix and $\nu^2$ is set such that uncertainty in the measurement and low-level noise are not amplified through the process of inverting $\mathbf{G}$. Methods to determine $\nu^2$ include the Morozov discrepancy procedure and the generalized cross validation procedure [16]. For this study, $\nu^2$ was chosen to be 70 dB below the largest eigenvalue of the cross-spectral matrix because of the known signal-to-noise ratio.

The hybrid builds on the standard Tikhonov regularization by defining a beamforming regularization matrix,

$$\mathbf{L}^{-1} = \left[ \mathrm{Diag}\left( \frac{\sqrt{\mathrm{diag}(\mathbf{Q_{CBF}})}}{\sqrt{\|\mathrm{diag}(\mathbf{Q_{CBF}})\|_\infty}} \right) \right]. \tag{6}$$

In Eq. (6), $\mathbf{L}^{-1}$ consists of a square matrix with elements formed from the individual source powers from $\mathrm{diag}(\mathbf{Q_{CBF}})$. Here, $\mathrm{diag}(\cdot)$ takes the diagonal elements of a matrix and $\mathrm{Diag}(\cdot)$ forms a diagonal matrix of these elements, $\|\cdot\|_\infty$ is the infinity norm, and $\sqrt{\cdot}$ is applied element-wise. The beamforming regularization matrix is an improvement to the standard regularization process because the Green function matrix is weighted by cross beamforming source powers to emphasize signals at the source region. Incorporating Eq. (6) into Eq. (5) and simplifying produces

$$\mathbf{q'} = \mathbf{L}^{-1}\left(\underline{\mathbf{G}}^{\mathbf{H}} \underline{\mathbf{G}} + \nu^2 \mathbf{I}\right)^{-1} \underline{\mathbf{G}}^{\mathbf{H}} \mathbf{p}, \tag{7}$$

where $\underline{\mathbf{G}} = \mathbf{G}\mathbf{L}^{-1}$, and $\mathbf{q'}$ is the estimated vector of source powers. Using Eq. (7), the hybrid method is developed such that

$$\mathbf{Q_{HM}} = \mathbf{q'q'^H} = \mathbf{L}^{-1}\left(\mathbf{J}\,\underline{\mathbf{G}}^{\mathbf{H}}\right)\mathbf{C}\left(\underline{\mathbf{G}}\,\mathbf{J}^{\mathbf{H}}\right)(\mathbf{L}^{-1})^{\mathbf{H}}, \tag{8}$$

where

$$\boldsymbol{J} = \left(\underline{\mathbf{G}}^{\mathbf{H}} \underline{\mathbf{G}} + \nu^2 \mathbf{I}\right)^{-1}. \tag{9}$$

Similar to the cross beamforming method, the hybrid method response, $\mathbf{Q_{HM}}$, is a matrix with auto and cross beamforming elements.

### 2.3 Generalized Inverse Beamforming

The improved generalized inverse beamforming method described by Dougherty [5] is distinct from cross beamforming in one primary point. As opposed to using a Green function to calculate the steering vector matrix in Eq. (4), the improved generalized inverse method uses the Moore-Penrose generalized inverse of the steering vector matrix, $\mathbf{G}^\dagger$ [5]. This is a more direct method for solving Eq. (2) and in practice can be calculated by taking the inverse of the singular value decomposition of $\mathbf{G}$ (where the decomposition is $\mathbf{G} = \mathbf{U\,\Sigma\,V^H}$). The inverse is then simply calculated by taking the inverse of the diagonal singular values matrix, $\mathbf{\Sigma}$. The result of the generalized inverse method is then

$$\begin{aligned} \mathbf{Q_{GINV}} &= \mathbf{G}^\dagger\, \mathbf{C}\, (\mathbf{G}^\dagger)^{\mathrm{H}} \\ &= \mathbf{V}\, \mathbf{\Sigma}^{-1} \mathbf{U}^{\mathrm{H}}\, \mathbf{C}\, \mathbf{U}\, \mathbf{\Sigma}^{-1} \mathbf{V}^{\mathrm{H}}, \end{aligned} \tag{10}$$

Because very small singular values are amplified under a reciprocation, regularization is necessary to determine an appropriate lower limit in the singular values. All values below this limit are replaced with a lower limiting value so as to bound the amplification of less-pertinent features of the Green function matrix. In this study, an appropriate cutoff was determined empirically to lie between 3-10 dB below the largest singular value, and a value of 7 dB was chosen here. The choice of cutoff levels can significantly alter the resultant field predictions, particularly in the low-level radiation regions. This choice allowed for a smooth source estimate as well as a smooth field estimate which did not contain additional spurious artifacts. This choice of cutoff value approximates that used by

Dougherty [5], who used a value of about 1.4 dB below the largest singular value.

### 2.4 Field Predictions

Where source benchmarks are not available, the ability of $\mathbf{Q}$ to predict field characteristics is an important measure of its success as an equivalent source model. $\mathbf{Q}$ is propagated for each of the methods by defining a new Green function, $\mathbf{G}_p$, that includes steering vectors for additional locations [5]. The cross spectral matrix of field pressures, $\mathbf{C}_p$, at those locations can by modelled using

$$\mathbf{C}_p = \left|\mathbf{G_p q}\right|^2 = \mathbf{G_p}\ \mathbf{Q}\ \mathbf{G_p^H}. \tag{11}$$

Levels are calculated by taking the magnitude the diagonal elements of $\mathbf{C}_p$ and are shown on a decibel scale. Furthermore, $\mathbf{C}_p$ provides the necessary information to calculate the coherence properties of the field. For reference location, $\vec{x}_{p_1}$, and another position $\vec{x}_{p_2}$, the coherence is calculated as

$$\gamma^2_{x_{p_1}x_{p_2}} = \frac{\left|\mathbf{C_p}\left(\vec{x}_{p_1}, \vec{x}_{p_2}\right)\right|^2}{\mathbf{C_p}\left(\vec{x}_{p_1}, \vec{x}_{p_1}\right)\mathbf{C_p}\left(\vec{x}_{p_2}, \vec{x}_{p_2}\right)}. \tag{12}$$

Because coherence is dependent on a reference location [11], coherence lengths provide a means of summarizing the spatial variation in the coherence [17]. Coherence length is defined as the distance from a reference location over which coherence is significant ($\gamma^2 \geq 0.5$). The ability of equivalent sources obtained from beamforming methods to predict coherence lengths is an important measure of the methods' success when applied to an extended, partially correlated source.

### 2.5 Wavepacket Source Model

A numerical study has been designed to test the ability of the different beamforming methods to obtain source properties and reproduce levels and coherence features of the sound field. The input for the beamforming methods is produced by a complex wavepacket source model that is extended, directional, and spans multiple wavelengths. The partially correlated nature of the source is simulated by combining multiple wavepackets, each with a different amplitude and wavenumber. This multiple-wavepacket model simulates the jet noise environment by broadening the directionality of the acoustic radiation and by providing a field that has spatially dependent, finite coherence lengths.

In this study, we adopt the wavepacket shape similar to the one described by Papamoschou [18], who modeled the pressure fluctuations on a cylindrical surface as an axisymmetric solution to the wave equation in cylindrical coordinates and provided convenient means to control for the growth, decay and wavenumber of the source. However, we make a slight adjustment to instead define element source strengths along the jet centerline for an acoustic volume velocity wavepacket, as

$$Q(z) = \tanh\left[\left(\frac{z}{b_1}\right)^{g_1}\right]\left\{1 - \tanh\left[\left(\frac{z}{b_2}\right)^{g_2}\right]\right\}e^{i\alpha z}. \tag{13}$$

Here, $\alpha$ is the spatial wavenumber (valid for $\alpha \leq k$), $b_1$ and $g_1$ determine the length scale and the rate of growth of the wavepacket amplitude, and $b_2$ and $g_2$ similarly determine the length scale and rate of decay of the wavepacket.

For a given acoustic wavelength, $\lambda$, a single wavepacket solution has been demonstrated to successfully simulate the strong directional properties of supersonic jet noise radiation [18-20]. However, because a single wavepacket is self-coherent, any resulting acoustic radiation is likewise completely coherent. On the other hand, a system of wavepackets, each with a different spatial wavenumber, $\alpha_i$, provides a set of self-coherent but mutually incoherent sources that generate a partially correlated sound field. The real part and magnitude of a multiple wavepacket source distribution used in this numerical study is represented in Fig. 1(a), where the properties have been defined as $b_1 = 5\lambda$, $b_2 = 3\lambda$, $g_1 = 3$, $g_2 = 1$, and $\alpha = k/2$, and where $k$ is the acoustic wavenumber. Thirty wavepackets (chosen to ensure a smoothly-varying field) differ in spatial wavenumber, which ranges between $0.1k \leq \alpha_i \leq 0.9k$, with an average wavenumber $\langle\alpha_i\rangle = k/2$. The different wavepackets [of which five are displayed in Fig. 1(a)] are weighted in amplitude such that greater weighting is given to wavepackets with a spatial wavenumber approaching $k/2$.

When this multiple-wavepacket source is propagated over a large plane using Eq. (11), the acoustic radiation displayed in Fig. 1(b) is obtained, where $x$ represents the horizontal distance from the jet centerline in terms of $\lambda$, and $z$ the downstream distance from the nozzle exit plane. Efficient radiation of this multiple-wavepacket source occurs because $\alpha \leq k$ causing highly directional radiation with the maximum occurring at the angle $\phi$ (defined normal to the positive $z$ axis), as

$$\phi = \sin^{-1}(\alpha/k). \tag{14}$$

In this example, $\alpha = k/2$, so $\phi = \sin^{-1}(1/2) = 30°$.

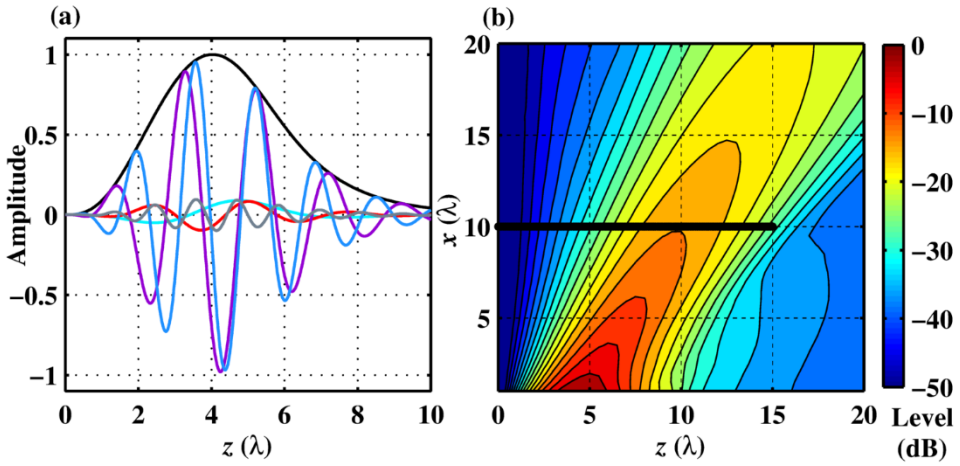


**Fig. 1 (a) Wavepacket magnitude and associated real parts for a source distribution consisting of multiple wavepackets with varying wavenumber. (b) The resultant radiated field and a black line indicating the array input for the beamforming algorithms.**

For the comparison of the beamforming methods, a simulated linear array with $\lambda/10$ element spacing is placed $10\lambda$ from and parallel to the source distribution [shown by the black line in Fig. 1(b)]. This geometry was chosen so as to model a typical one-dimensional full-scale jet noise measurement that can include a high density of microphones but cannot place microphones in the far-downstream direction (large $z$) due to the increasing jet width and other obstacles such as jet blast deflectors. The lack of input information generally produces greater errors in radiation levels far downstream of the source. Additionally, to provide the opportunity to evaluate the behavior of the beamforming algorithms in the presence of measurement noise, a noise floor was added to the input such that the minimum level at all field locations is 70 dB below the maximum level measured at the line array.

## 3 Results

Cross beamforming (CBF), the hybrid method (HM) and generalized inverse beamforming (GINV) are all applied to the sound field generated on the linear array from the multiple-wavepacket source described in Sec 2.5. The resulting equivalent source distributions contained in **Q** are then used to predict the levels in the geometric near field of the source using Eq. (11). They are also propagated to a far-field arc to predict the levels and coherence lengths. When compared with the benchmarks, these predictions indicate the utility of each method when applied to the characterization of an extended, partially correlated source distribution.

The three beamforming methods are applied to complex pressures at the near-field, linear array [shown in Fig. 1(b)]. The resulting source level and coherence length estimates are given in Fig. 2(a) and Fig. 2(c) respectively, with the corresponding errors provided in Fig. 2(b) and Fig. 2(d). Due to the high-density array design, all three methods agree well with the benchmark source levels, with errors only becoming significant below about 20 dB from the maximum source level. In this region, errors are most prominent in the HM results, which underpredict the source levels by up to 5 dB in the low-amplitude regions. This may result from the method's regularization process which emphasizes the signal in the high source level region. The CBF and GINV results agree with the benchmark to within 1 dB to about 30 dB below the maximum source levels.

Coherence length, described in Section 2.4, is defined here as the distance from a reference location to a point upstream ($-z$ direction) where coherence drops below 0.5. The benchmark source coherence length is shown as a black solid line in Fig. 2(c). For reference locations where the coherence is not less than 0.5 at the edges of the source reconstruction region, the coherence length is not defined. The coherence lengths from the beamforming results are plotted in Fig. 2(c) and show general agreement with the benchmark values over the measureable range. However, the relative error in Fig. 2(d) shows that results vary from the benchmark by as much as 40%, particularly at the edges of the source region. In general, the variation in the coherence estimates is greatest with HM results. This is likely due to the HM regularization that produces less stringent constraints on the source properties. The GINV results have less variation—within 10% if the edges of the estimate

region are disregarded. The CBF results are similar to GINV, except with slightly larger errors.

These results indicate that within the source region, cross beamforming methods can predict the source coherence properties to within about 10% accuracy, although errors exist, particularly at the edges of the source distribution. Only a few studies have previously considered the coherence properties of a source estimate obtained from beamforming analyses. For example, a study by Papamoschou [21] was conducted in which beamforming results from a far-field array were used in correlation calculations with flow-field parameters at the source region measured using optical deflectometry techniques. He measured significant correlation ($> 0.1$) between the beamformed pressure distribution and the flow measurements over the span of the flow. Similarly, cross beamforming and DAMAS-C were applied to measurements of an F-22A aircraft in the geometric near-field to predict coherence information across the source region [11]. Appreciable source coherence was found with coherence lengths spanning multiple wavelengths, particularly at low Strouhal numbers. This study highlights the capabilities of improved beamforming methods to estimate coherence properties of the source reconstruction.

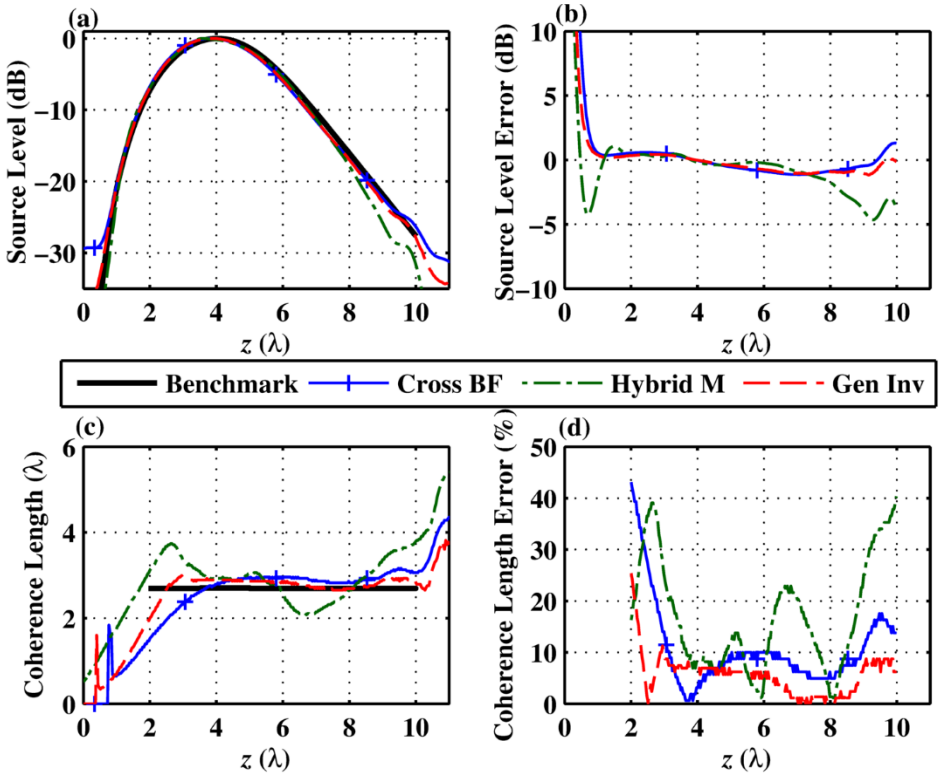


**Fig. 2. Beamforming results of the wavepacket source for three methods along with benchmarks: (a) source levels and (b) level error; (c) source coherence lengths and (d) corresponding error.**

The equivalent source distributions generated by the beamforming results are used to predict the corresponding acoustic field over a large spatial aperture. The predicted field from the beamforming results is shown in Fig. 3(a) - Fig. 3(c), and the fields are compared with the benchmark field in Fig. 1(b) to produce error plots in Fig. 3(d) - Fig. 3(f). Similar to the source estimates, each of the predicted fields show general agreement with the benchmark field levels, particularly in the region spanned by the linear array. In this region, the predicted field using the CBF results has errors within about 1 dB. Errors in this region are even smaller for results from HM and GINV, with variations across most of the field within 0.1 dB of the benchmark levels. However, in regions not spanned by the array ($z > 15\lambda$ at the array), larger errors are present. The GINV and CBF results significantly underestimate the downstream levels, while the corresponding HM results are overestimated but much closer to the benchmark levels. One possibility for the improved downstream results is the slightly compressed nature of the HM source [see Fig. 2(a)] that creates a more omnidirectional radiator.

Alternatively, because the HM places greater emphasis on the source region due to the beamforming regularization matrix (see Section 2.2), the source signals are amplified, including radiation from wavepackets which have directivities predominantly beyond the span of the linear array. HM results also include additional spurious artifacts which radiate upstream of the linear array and which are greatly affected by the regularization procedure. It is likely that the regularization process for the HM method can be optimized to reduce these artifacts.

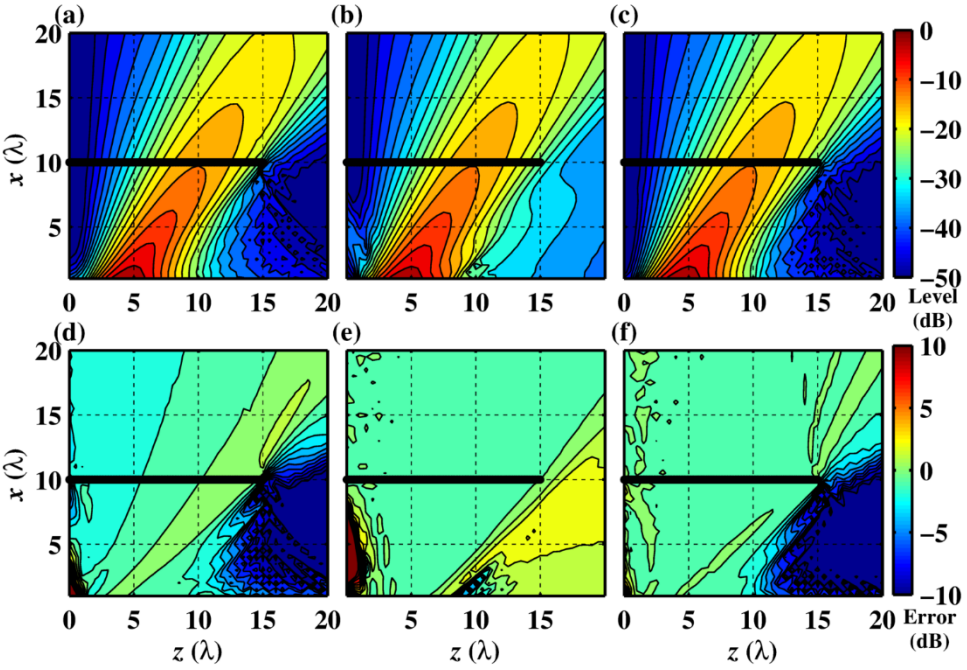


**Fig. 3. Predicted acoustic field levels in the vicinity of the wavepacket source, generated from source estimates using (a) cross beamforming, (b) hybrid method, and (c) improved generalized inverse beamforming. The corresponding level errors of each field are shown in (d)-(f).**

When propagated to the far field, the levels and coherence lengths estimates derived from the beamforming results can also be compared with benchmark values at a large distance from the source region. Pressures from the numerical source are calculated at $100\lambda$ from the origin in a polar pattern, and the levels and coherence lengths, in degrees, are shown (black solid line) in Fig. 4(a) and Fig. 4(c). The values are oriented such that the 0° is perpendicular to the $z$ axis, and the levels at all angles shown are well above the noise floor. Predicted far-field levels are shown for each beamforming source method alongside the benchmark values. As shown, the levels from each method are within 1 dB for values from $0° \leq \theta \leq 50°$, and HM and GINV results are within 0.1 dB over much of the measurement. At shallower angles (i.e., farther downstream), the CBF and GINV results drop off smoothly at angles outside the maximum radiation region while the HM levels are within 3 dB of the benchmark, likely for the same reasons that describe the downstream HM-predicted near-field levels in Fig. 3(b).

Estimated and actual coherence lengths across the far-field locations are shown in Fig. 4(c). While the far-field levels predicted by each beamforming method agree well with benchmark values, the coherence lengths have more variation. All predicted lengths are accurate to within about 10% of benchmark values for far-field angles spanned by the linear array. However, coherence lengths are significantly overpredicted at downstream angles beyond the span of the linear array. The HM results contain variation up to 50% beyond the benchmark values, while CBF and GINV results show relative errors exceeding 200-300% of the benchmark values. This is different from the source coherence length errors in Fig. 2, where HM results showed greater deviation from the benchmark. Thus, while the GINV regularization procedure produces an improvement from the CBF results in predicting both the source and field levels and coherence lengths, the HM regularization is shown to better reproduce the radiation properties in the field.

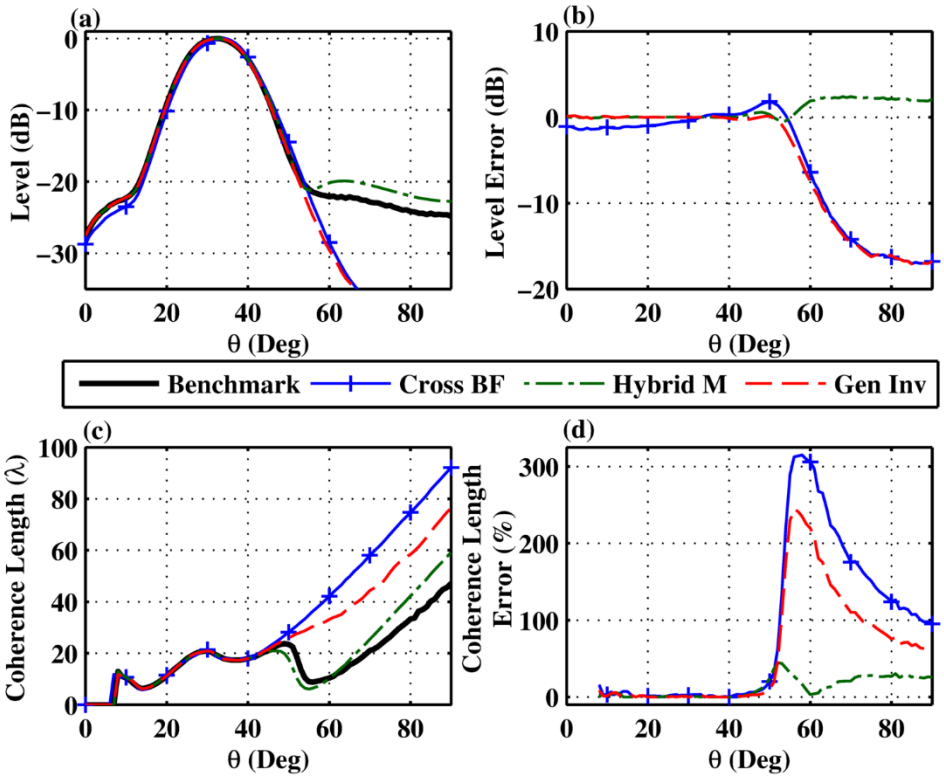


**Fig. 4 Far-field predicted (a) source levels and (c) coherence lengths, using beamforming methods and plotted alongside benchmark values. Level and coherence length errors are plotted alongside in (b) and (d).**

## 4 Conclusions

Multiple advanced beamforming techniques have been applied to a numerical case study of an extended, partially correlated source with levels and coherence features that are representative of a supersonic jet noise measurement. Cross beamforming [8], the hybrid method [9], and improved generalized inverse beamforming [5] have been compared. Source level and coherence estimates were obtained using input from a high-density linear array placed in the geometric near field of a multiple-wavepacket numerical source. While cross beamforming and the improved generalized inverse method predicted the source features to high accuracy, the hybrid method produced small deviations from benchmark values in the low-amplitude regions of the source. These source estimates were additionally used to predict the acoustic levels in the near and far-fields, as well as coherence properties. In the geometric near-field, both the generalized inverse method and the hybrid method produced levels which were within 0.1 dB of benchmark values throughout the angular aperture spanned by the array. The hybrid method also produced estimates beyond the span of the linear array which were within 5 dB of the benchmark, although in the upstream direction additional artifacts were present. When propagated to the far field, levels estimated by each method showed agreement within 1 dB of benchmark levels in the regions spanned by the near-field measurement array.

While it is common to only consider level-based analyses, for an extended, partially correlated source, the coherence properties are equally important, thus allowing for more complete and accurate modeling. Coherence lengths have been applied here to demonstrate how the previously described beamforming methods are useful to reproduce the coherence of both the field and the source information. The coherence lengths predicted at the source were in general agreement with the benchmark values, although results from improved generalized inverse beamforming were accurate to within 10% over the majority of the source region. When predicting the far-field coherence lengths, all equivalent source models produced results within about 10% of benchmark values over the aperture spanned by the near-field linear array. The success of the beamforming results to predict extended, partially correlated sources has direct application to full-scale jet noise measurements. Accurate source estimates provide greater insight into the properties of the source, which, when combined

with flow parameters provides physical insight into jet noise source mechanisms. These models can also be used to predict near and far-field noise levels.

Regularization techniques and the choice of parameters which amplify or repress low-level artifacts are an important consideration when using beamforming algorithms, and, in many cases, prior knowledge of the source distribution is required to empirically determine artifacts present in the results. A part of the difficulty in producing accurate beamforming results is related to the utilization of and choices regarding regularization methods and associated parameters. Both regularization-based beamforming techniques had high degrees of variability in the resultant predicted fields based on the selection of regularization parameters, although the improved generalized inverse method was more sensitive. Further work applying more robust regularization techniques should allow for less variation in the beamforming results, particularly when more noise is present. For example, the generalized cross validation technique used in modified Tikhonov regularization [16] may improve the regularization parameter selection process. Additionally, the merging of methods by incorporating the beamforming regularization matrix to improved generalized inverse beamforming could further enhance the beamforming results. Finally, deconvolution techniques (e.g., DAMAS-C) and proper grid selection along the source region reduce artifacts caused by array geometry, particularly for arrays which do not span the source region. These improvements should produce equivalent source models with increased accuracy that enable more complete and accurate predictions of the radiated field.

## REFERENCES


[1] M. H. Blaine, K. L. Gee, and B. N. Tracianne, "Application of beamforming methods to extended partially correlated sources," Proceedings of 2016 Berlin Beamforming Conference, Berlin, Germany, http://www.bebec.eu.

[2] D. V. Affairs, "Annual Benefits Report Fiscal Year 2011," 2012.

[3] S. S. Lee and J. Bridges, "Phased-Array Study of Dual-Flow Jet Noise: Effect of Nozzles and Mixers," AIAA Paper 2006-2647, 2006.

[4] T. F. Brooks and W. M. Humphreys, "A deconvolution approach for the mapping of acoustic sources (DAMAS) determined from phased microphone arrays," J. Sound Vib. **294**, 856-879 (2006).

[5] R. P. Dougherty, "Improved generalized inverse beamforming for jet noise," Int J Aeroacoust **11**, 259-290 (2012).

[6] P. Sijtsma, "CLEAN based on spatial source coherence," Int J Aeroacoust **6**, 357-374 (2007).

[7] B. M. Harker, K. L. Gee, T. B. Neilsen, A. T. Wall, and M. M. James, "Wavepacket modeling and fullscale military jet noise beamforming analyses," AIAA Paper 2016-2129, 2016.

[8] T. F. Brooks and W. M. Humphreys Jr, "Extension of DAMAS phased array processing for spatial coherence determination (DAMAS-C)," AIAA Paper 2006-2654, 2006.

[9] T. Padois, A. Berry, P.-A. Gauthier, and N. Joshi, "Beamforming matrix regularization and inverse problem for sound source localization : application to aero-engine noise," AIAA Paper 2013-2212, 2013.

[10] S. R. Venkatesh, D. R. Polak, and S. Narayanan, "Beamforming algorithm for distributed source localization and its application to jet noise," AIAA J. **41**, 1238-1246 (2003).

[11] B. M. Harker, T. B. Neilsen, K. L. Gee, A. T. Wall, and M. M. James, "Spatiotemporal Correlation Analysis of Jet Noise from a High-Performance Military Aircraft," AIAA J. (Accepted Dec. 2015).

[12] T. Suzuki, "L1 generalized inverse beam-forming algorithm resolving coherent/incoherent, distributed and multipole sources," J. Sound Vib. **330**, 5835-5851 (2011).

[13] Y. Du and P. J. Morris, "Numerical simulation of the effect of a low bypass cooling stream on supersonic jet noise," AIAA Paper 2014-1402, 2014.

[14] R. P. Dougherty, in *Aeroacoustic Measurements* (2002), pp. 62-97.

[15] E. Sarradj, "Three-Dimensional Acoustic Source Mapping with Different Beamforming Steering Vector Formulations," Advances in Acoustics and Vibration **2012**, (2012).

[16] E. G. Williams, "Regularization methods for near-field acoustical holography," J. Acoust. Soc. Am. **110**, 1976-1988 (2001).

[17] A. T. Wall, M. D. Gardner, K. L. Gee, and T. B. Neilsen, "Coherence length as a figure of merit in multireference near-field acoustical holographya)," J. Acoust. Soc. Am. **132**, EL215-EL221 (2012).

[18] D. Papamoschou, "Wavepacket modeling of the jet noise source," AIAA Paper 2011-2835, 2011.

[19] R. Reba, S. Narayanan, and T. Colonius, "Wave-packet models for large-scale mixing noise," Int J Aeroacoust **9**, 533-558 (2010).

[20] P. Morris, R. Dougherty, C. Nelson, A. Cain, and K. Brentner, "Wavepacket noise source model for microphone array data analysis of hot supersonic jets," J. Acoust. Soc. Am. **134**, 4127-4127 (2013).

[21] D. Papamoschou, P. J. Morris, and D. K. McLaughlin, "Beamformed flow-acoustic correlations in high-speed jets," AIAA Paper 2009-3212, 2009.